

M. P. Mughal · H. Fawad · R. Mufti

## Parametric thermal analysis of a single molten metal droplet as applied to layered manufacturing

Received: 5 October 2004 / Accepted: 14 June 2005 / Published online: 12 August 2005  
© Springer-Verlag 2005

**Abstract** In the present study a parametric thermal analysis of a single molten metal droplet deposited on a large substrate has been performed with application to various solid freeform fabrication (SFF) processes employing droplet-based deposition. Simulation is conducted to investigate the effect of droplet shape, substrate thermal properties, substrate size and thermal boundary conditions of substrate base on the cooling rate of the droplet and the substrate. It is found that droplet shape and substrate thermal properties have significant effect only on the solidification time, whereas the steady-state conditions vary significantly with all the process parameters studied.

### Nomenclature

$L$	Droplet contact length (m)
$C_p$	Specific heat (J/Kg K)
$\Delta E$	Change in energy (J)
$Fo$	Dimensionless fourier number (–)
$H$	Height of spherical cap (m)
$K$	Thermal conductivity (W/m K)
$h_{sf}$	Heat of fusion (J/Kg)
$n$	Unit normal vector
$R$	Radius of sphere (m)
$st$	Substrate thickness (m)
$t_s$	Solidification time (s)
$T$	Temperature (K)
$V$	Volume of spherical cap (m <sup>3</sup> )
$X$	Location of melting front (m)

### Greek symbol

$\alpha$	Thermal diffusivity (m <sup>2</sup> /s)
$\theta$	Contact angle (Radians)
$\rho$	Density (Kg/m <sup>3</sup> )
$\tau$	Time (s)

### Subscript

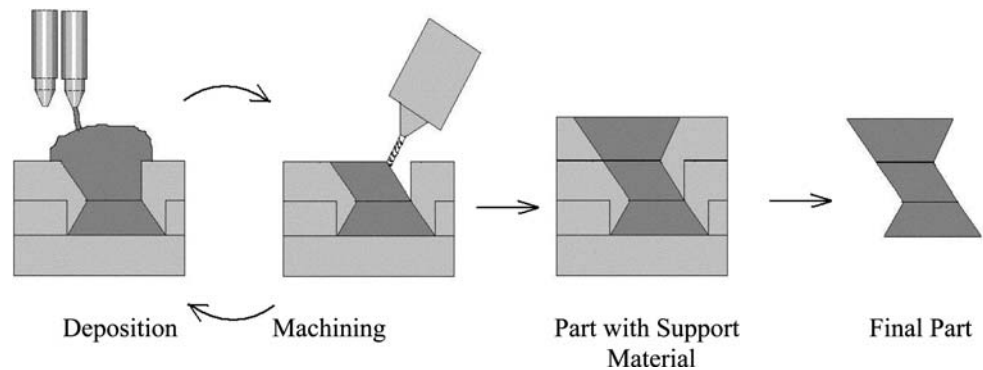
$s$	Solid domain
$l$	Liquid domain

## 1 Introduction

In rapid prototyping (RP) or solid freeform fabrication (SFF) process, a computer model of a part is sliced into layers and this layer-wise geometric data are then fed into a deposition machine to produce parts. These parts are built up layer by layer. In ordinary SFF processes like stereo lithography, 3D printing and fused deposition modeling, layers are built up either by polymer curing or by successive deposition of molten polymer to create a non-functional model of the part. Even though the above-mentioned processes have produced a significant impact on design and manufacturing, none have the capability to directly produce fully functional parts (parts of high structural integrity, i.e. mainly metal parts) with excellent dimensional tolerances that could be used in operational systems [1]. In view of the above limitations of conventional SFF techniques, a number of other methods like shape welding and 3D welding have been employed. They produced parts with high material strength but the control of geometrical tolerances is difficult, moreover, geometrical complexity is limited and finishing operations are required to produce high-performance parts. To address these challenges, a new method, shape deposition manufacturing (SDM), is

M. P. Mughal (✉) · H. Fawad · R. Mufti  
Faculty of Mechanical Engineering,  
GIK Institute of Engineering Sciences and Technology,  
Topi, NWFP, Pakistan  
E-mail: mughal@giki.edu.pk  
Tel.: +92-938-71858

Fig. 1 SDM, general layout



being developed at Stanford and Carnegie Mellon University. The SDM combines the benefits of SFF (quickly planned, independent of geometry), CNC milling (accuracy and precision with good surface quality), weld-based deposition (superior material properties) and shot peening (control of internal stress buildup).

The basic steps for building parts with shape deposition are depicted in Fig. 1. To form each layer the growing shape is transferred to several processing stations. First, the material for each layer is deposited as a near-net shape using a novel weld-based deposition process called microcasting. The part is then transferred to a shaping station, such as a five-axes CNC milling machine, where material is removed to form the net shape. In the next step the part is then transferred to the deposition station, where complementary shaped, sacrificial support material is also deposited and the support material is removed to produce the desired part.

The metal deposition process used within SDM is called microcasting, which is able to create fully dense metal layers with controlled microstructure. It involves depositing discrete molten metal droplets produced by melting feedstock wire using a conventional GMA welding torch. The size of these droplets ranges from 1 to 5 mm [2], fall through an inert environment on to a substrate, where they melt the substrate and solidify to become part of the substrate. Important issues in the production of high-quality parts manufactured with microcasting involve controlling the substrate remelting and droplet/substrate cooling rates.

The existing literature on the thermal modeling of the microcasting process is very limited; some aspects of microcasting are similar to the thermal spraying, welding and casting processes. Research in welding and casting is mostly focused on the build-up of residual stresses and distortions, whereas the research in thermal spray has been focused largely on the modeling of droplet impingement, spreading and solidification, on the level of single droplet by Trapaga et al. [3], Bertagnolli et al. [4], multiple droplets by Kang et al. [5] and an array of evaporating injected droplets by Xin and Megaridis [6]. In all these studies the solidification heat transfer was modeled by using an empirically determined heat transfer coefficient between the substrate and droplet. Substrate remelting caused by micro-droplet

deposition was modeled by Attinger and Poulikakos [7]. A threshold Biot number was determined above which the substrate melt boundary advances in a similar fashion. The effects of impact velocity, thermal and hydrodynamic conditions were studied with respect to substrate remelting. Numerical simulation to predict droplet shape in reduced gravity was performed by Haferi et al. [8] with good experimental verification. It was reported that Froude number plays an important role in the final equilibrium shape, while the solidification time shows a non-intuitive trend. Numerical modeling of droplet pileup was performed by Haferi and Poulikakos [9], which gives good results for cases where inertia effect dominates.

The reference works discussed are relevant to the modeling of the thermal spray process. The microcasting process numerically modeled in this paper differs significantly from the traditional spray process in the size, temperature and velocity of the droplet. In microcasting the size of the droplet ranges from 1 to 5 mm and they fall through an inert environment at a rate of several droplets per seconds. While in the thermal spray process the droplet size is about 100  $\mu\text{m}$ , propelled as high-velocity mist toward the substrate, the microcasting droplet has a large volume-to-surface area ratio; therefore the droplet is several 100° above the melting temperature. In contrast, the spray droplet is deposited near or below the melting point, therefore the referred work cannot be used directly for the modeling of microcasting process.

By numerical modeling and experimental verification of the MD spray shape deposit process, Amon et al. [10] reveals that a 1D model can correctly predict the substrate remelting and to some extent the solidification time. The model was tested for a number of multi-material combinations and it was observed that remelting can be achieved if the droplet impact temperature is near the material vaporization temperature for an unheated substrate or several 100° above the melting point for a preheated substrate. A 1D model of a microcasting droplet was developed by Amon et al. [11], to predict the location of the melting front. The numerical results were compared with an analytical solution and it was found that the analytical solution compared well during the initial cooling phase. Drop-

let-level modeling of the microcasting process has been performed by Chin et al. [12], using a cylindrical droplet on a large cylindrical substrate to study the solidification behavior and buildup of residual stresses. It was found that substrate preheating will decrease the cooling rate of the droplet and will eventually affect the buildup of residual stress; this study was further extended to take into account successive deposited layers and columns of droplets [13] and adjacent droplets [14]. In order to incorporate the dynamic effect of droplet spreading, the microcasting model was modified by using an effective liquid conductivity Zarzalejo et al. [15], obtained by multiplying the liquid conductivity by a conductivity multiplier, to account for the fluid motion near the droplet and substrate interface. The multiplier was quantified by heat balance at the droplet and substrate interface. The model was verified by metallographic examination of remelting depth and thermocouple measurement was performed for the determination of deposited material temperature history. It was found that for stainless steel a multiplier of five gives good agreement with experimental measurements. Schmaltz et al. [16] reported that changes in the initial droplet temperature within the range found in microcasting have no effect on the droplet-cooling rate during solidification. On the other hand, it is found that a 2,000°C copper (C) droplet induces a sixfold increase in the remelting depth compared to a 1,800°C droplet. Therefore, metallurgical bonding between layers can be improved by increasing the initial droplet temperature without affecting the final microstructure. It is found that preheating the substrate decreases the droplet-cooling rate during solidification. However, this effect diminishes towards the droplet top. Numerical simulations also reveal that the region close to the droplet/substrate interface experiences cooling rates that are an order of magnitude higher than those at the droplet top region. Therefore, it is possible to control this rapid cooling and obtain a more homogeneous microstructure throughout the droplet domain by increasing the initial temperature of the substrate. Numerical results also show that preheating the substrate facilitates the remelting process. The droplet solidification time is delayed when either the initial droplet temperature or the substrate temperature is increased. This is relevant for successive droplet deposition since a better interlayer bonding is achieved when a droplet is deposited overlapping a previously deposited droplet that has not solidified completely.

Results for different combinations of C and stainless steel show that droplets deposited on C substrate experience higher cooling rates during solidification than droplets deposited on stainless steel. When using C as a sacrificial material for building stainless steel artifacts, preheating of C is desired to obtain homogeneous microstructure in the steel part. In addition, remelting is less likely to occur when steel is deposited over C. The use of C as a sacrificial material is recommended since C can be easily removed while maintaining a good stainless steel surface quality.

In SFF processes the buildup of residual stresses and deformations due to successive material deposition is a major problem since it results in loss of tolerance, warpage and delamination. In SFF processes using welding as a method of metal deposition, the problems can be much more serious since welding causes residual stresses of the order of yield strength due to the large amount of heat input into the system and the rate at which the deposition and the substrate cools down. Theoretically, by controlling or slowing down the cooling process these problems can be reduced to the level where parts of suitable tolerances and strength can be achieved.

The present work is actually an extension of the modeling reported by Chin et al. [12–14] who studied the solidification time and steady-state time for a cylindrical microcasting droplet, whereas a different set of parameters have been studied in the present work. The main aim of this work is to develop a thermal model in order to study the effect of various process parameters like droplet shape based on contact angles, as shown in Fig. 2, substrate thermal properties, substrate size and the boundary conditions imposed at the base of the substrate, on the cooling rate of the droplet and the substrate and its effect on the solidification time of the droplet as well as the time required to achieve the steady-state conditions.

The angle formed at a point on the line of contact of three phases, as shown in Fig. 2, of which at least two are condensed phases and taken from the liquid side, is called the contact angle. One of the phases must be a liquid, another phase may be solid or liquid and the third phase may be gas or liquid. The contact angle can change for a particular interface either due to impurities present in the liquid phase or due to surface properties, e.g. the surface roughness of the solid phase and other thermal and hydrodynamic factors. In this study these factors are not discussed, rather the effects of various

**Fig. 2** Contact angle

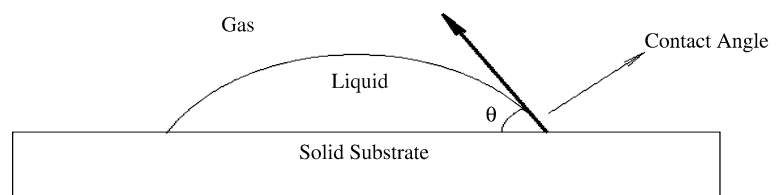
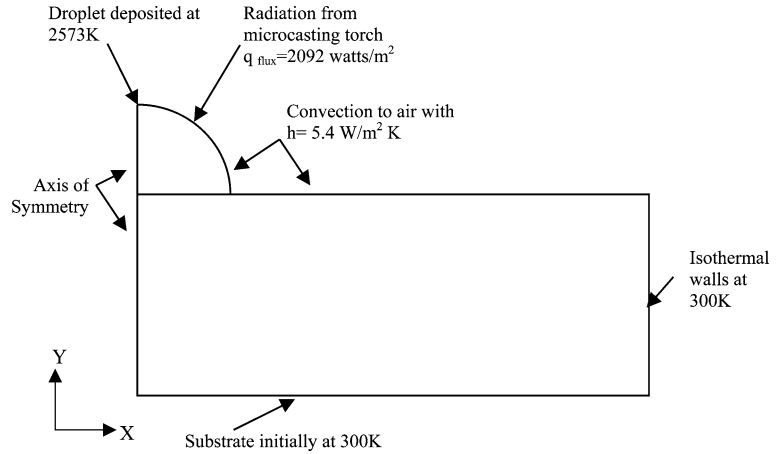


**Fig. 3** Schematic of droplet and substrate interface



process parameters on the thermal behavior of the droplet substrate domain have been analyzed.

## 2 Model description

In this analysis a 2D axisymmetric thermal model of the spherical droplet deposited over a cylindrical substrate is presented. The actual process of deposition is a 3D problem with successive droplets being deposited in series resulting in substrate preheating and edge effects. In order to understand the effect of various parameters, independently, the effect of parameters like preheating and edge effect should be removed, which is why a single droplet deposited in the center of a large substrate is analyzed. The geometry of the model along with the boundary conditions is shown in Fig. 3. The geometry of the droplet is approximated as a spherical cap with dimensions like contact length, height of the droplet and radius of curvature determined using the equation from analytical geometry of a spherical cap. The volume of the spherical cap is similar for all the contact angles and

is equal to the volume of the cylindrical droplet as studied by Chin et al. [12]. The geometry of the spherical cap is shown in Fig. 4 with all the relevant dimensions.

The equations used to calculate the volume of the spherical cap is given as:

$$V = \pi H \frac{(3L^2 + H^2)}{6}. \quad (1)$$

In terms of the contact angle,  $\theta$

$$\sin \theta = \frac{(R - H)}{R}. \quad (2)$$

For different contact angles, keeping the volume as constant the dimensions,  $L$  and  $H$ , shown in Fig. 4 are calculated. The geometry of the substrate is cylindrical with the droplet deposited on the top center of the cylinder.

The effect of droplet spreading on heat transfer is ignored since the spreading is a precursor to droplet solidification [11]. This assumption is justified for the microcasting process since the size of the droplet is much larger than the size of the droplet used in thermal spraying, where the droplet spreading is a dominant feature. Deposition of new material on existing layers results in the remelting of the top of previous layers causing an intimate bond and therefore the thermal contact resistance is ignored. The effect of under cooling during solidification is ignored due to the relatively large size of the droplet. The radius of the substrate is chosen to be much larger than the contact length of the droplet, so that the heat transfer from droplet to substrate does not influence the sides of the substrate and they are kept at fixed temperature, apart from the top of the substrate where a convective boundary condition along with heat flux from microcasting torch is imposed. The top of the droplet is also exposed to radiation heat flux from the torch as well as the convective heat transfer to the environment. The temperature of the environment, above the droplet, is taken at 323 K, higher than the room temperature of 300 K due to the presence of radiation from the microcasting torch. The interface

R= Radius of Sphere  
L=Contact Length  
H=Droplet Height  
 $\theta$  = Contact Angle

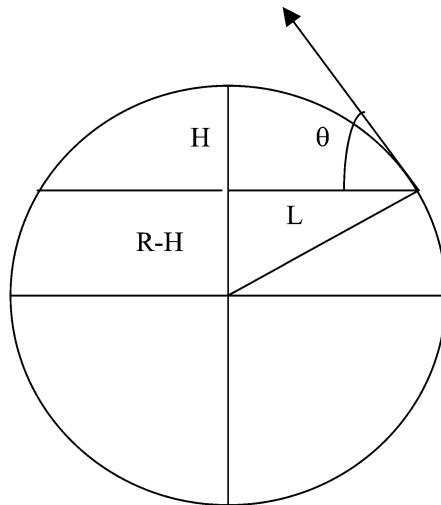


**Fig. 4** Spherical cap geometry

between the droplet and the substrate is assumed to be at the melting temperature. The solidification of the droplet is completed when the temperature anywhere within the droplet does not exceed the solidus temperature and the steady state is determined by the room temperature.

### 3 Governing equations

#### 3.1 Thermal modeling

The energy balance equation for any arbitrary domain is given as:

$$\Delta E = \text{Net energy into } CV + \text{Heat generation.} \quad (3)$$

Using the above principle and the Fourier law of heat conduction the differential form of the conservation law for a 2D domain can be written as:

$$\rho_i(T)C_{pi}(T)\frac{\partial T_i}{\partial t} = \frac{\partial}{\partial x_i}\left(K_i(T)\frac{\partial T_i}{\partial x_i}\right) + \frac{\partial}{\partial y_i}\left(K_i(T)\frac{\partial T_i}{\partial y_i}\right), \quad (4)$$

where  $i=1$  represents liquid region and  $i=2$  represents solid region.

Equation 2, is actually two equations; therefore the equations are linked by means of an interface equation Eq. 3, derived at the interface of liquid–solid regions, which is given as

$$K_s \frac{\partial T_s}{\partial n} - K_l \frac{\partial T_l}{\partial n} = \rho h_{sf} \frac{\partial X}{\partial t} \quad (5)$$

### 4 Material model

Temperature-dependent material properties of a mild steel (MS) droplet are used in this analysis while the substrate is assumed to be of MS and C for different studies. The material model for MS is adopted from Karlson and Josefson [17], Lide [19], and Chin et al. [12] with some extrapolation and simplification. The phase change has been modeled by taking a solidus temperature of 1,738 K and a liquidus temperature of 1,788 K, while for pure C substrate the melting temperature is

**Table 1** Thermal properties of mild steel

Thermal conductivity (W/m <sup>2</sup> K)					
Temperature (K)	273	373	673	1073	1723
$K$	40.3	39.5	37.2	26.9	33.1
Density (Kg/m <sup>3</sup> )					
Temperature (K)	300	550	800	1000	1300
$\rho$	7882	7715	7548	7415	7215
Specific heat (KJ/Kg K)					
Temperature (K)	273	888	1013	1213	1738
$C_p$	441	580	600	635	712
Latent heat (KJ/Kg, $L_f$ )	272				

**Table 2** Thermal properties of copper

Thermal conductivity (W/m <sup>2</sup> K)				
Temperature (K)	300	400	800	1000
$K$	398	392	371	357
Density (Kg/m <sup>3</sup> )				
Temperature (K)	300			
$\rho$	8910			
Specific heat (KJ/Kg K)				
Temperature (K)	298	873	1073	1273
$C_p$	385	442	462	482
Latent heat (KJ/Kg, $L_f$ )	207			

taken to be 1,357 K. The thermal properties of MS and C are given in Table. 1 and 2, respectively.

### 5 Model geometry and boundary conditions

The geometry of the 2D model consists of a rectangular substrate and that of the droplet is a spherical cap. The dimensions of the droplets depend upon the contact angle which is varied from 5 to 90° while keeping the volume of the droplet constant equal to that of the base case Chin et al. [12]. The other dimensions are calculated based on contact angle and volume. As far as the substrate is concerned its thickness varied from 10 to 4 mm while the diameter of the substrate is kept constant at 21 mm. The typical values of microcasting are temperature of 300 K for the substrate and 2,573 K for the droplet, while that of the environment is taken to be at 323 K. The radiation heat transfer from the top of the droplet to the atmosphere is neglected since the droplet remains at a high temperature for a very short period. A heat flux of 2,092 W m<sup>-2</sup> is imposed on the top of the droplet and substrate, simulating the radiation heat flux from the overhead microcasting torch. The convective heat transfer coefficient is taken to be 5.4 W m<sup>-2</sup> K<sup>-1</sup>, which is a typical value for free convection from a horizontal surface. Numerically the heat flux and convection coefficient have been adopted from Chin et al. [13]. The centerline of droplet and substrate acts as the axis of symmetry hence the heat flux across the edge is put to zero, other boundary conditions are shown in Fig. 3.

### 6 Finite element model

The finite element method is used to solve the non-linear transient 2D heat conduction equation for the coupled droplet–substrate domain; with the constitutive equation, which is the Fourier law of heat conduction. A commercial finite element code ANSYS is used to solve the problem and for post-processing. A plane four-noded element with axisymmetric feature and without mid-side nodes is used for the simulation of all the cases. A quadrilateral element is used for the substrate region

while a triangular element is used for the droplet region since the triangular element can model the curve geometry better. A biased mesh is used in all the analysis with a smaller element size near regions of large temperature gradients like droplet–substrate interface and axis of symmetry, while coarse mesh is used near the edges of the substrate. The process is very much mesh sensitive, therefore a number of test runs were made by altering the mesh size and the time step size until the solution was insensitive to the spatial and temporal discretization. In finite element analysis the temperature is continuous from one element to another but the heat flow is discontinuous. This is referred to as the thermal energy error. The thermal energy errors have been reduced to less than 5% and in regions near the droplet–substrate interface. A Newton Raphson method is applied to solve the non-linear problem. The modeling of phase change is important and in literature a number of different methods have been adopted for the modeling of solidification [18], but in this study an enthalpy method is used. During the phase change part of the solution, a smaller time step is used to capture the phenomena with more accuracy.

## 7 Model validation

Due to a lack of published results for thermal analysis of the microcasting process with spherical droplet, the present model has been verified with a similar model [12] by changing the spherical droplet to a cylindrical droplet and then predicting the solidification time. It has been found that the two models not only predict similar solidification time but the transient temperature distribution is also similar. The solidification time and steady-

state time as predicted by Chin et al. [12] is 0.174 and 11 s while the present model estimation is 0.16 and 10.8 s, respectively.

## 8 Results

The numerical simulations of combined droplet and substrate heat transfer are performed using finite element method (FEM). The main aim of the simulation was to estimate the effect of different process parameters like droplet shape defined by contact angle, substrate size, properties and substrate thermal boundary conditions, on solidification time of droplet and on the time required to obtain steady-state conditions. As shown in various graphs, MS–C line represents a MS droplet on C substrate, while MS–MS line represents a MS droplet on MS substrate; ISO represents an isothermal base while ADB represents an adiabatic base. The contact angle and substrate thickness are presented in degrees and millimeters, respectively.

Figure 5 shows the time temperature history of a point, located at the top of the droplet along the centerline, for different contact angles. The significance of this point is that the droplet solidification is completed when the melting front reaches this point. The flat portion of the graphs, around 1,788 K, represents the period when the phase change is taking place and the width of the flat portion is the time required for a particular droplet shape to release its latent heat. It is evident that the time required to change phase depends on the contact length; so for droplets with small contact angles the phase change is very rapid while for droplets with large contact angles this time is much longer.

The substrate acts as a large heat sink as soon as the droplet comes in contact with the substrate. The effect of

**Fig. 5** Time history response of droplet top for various contact angles

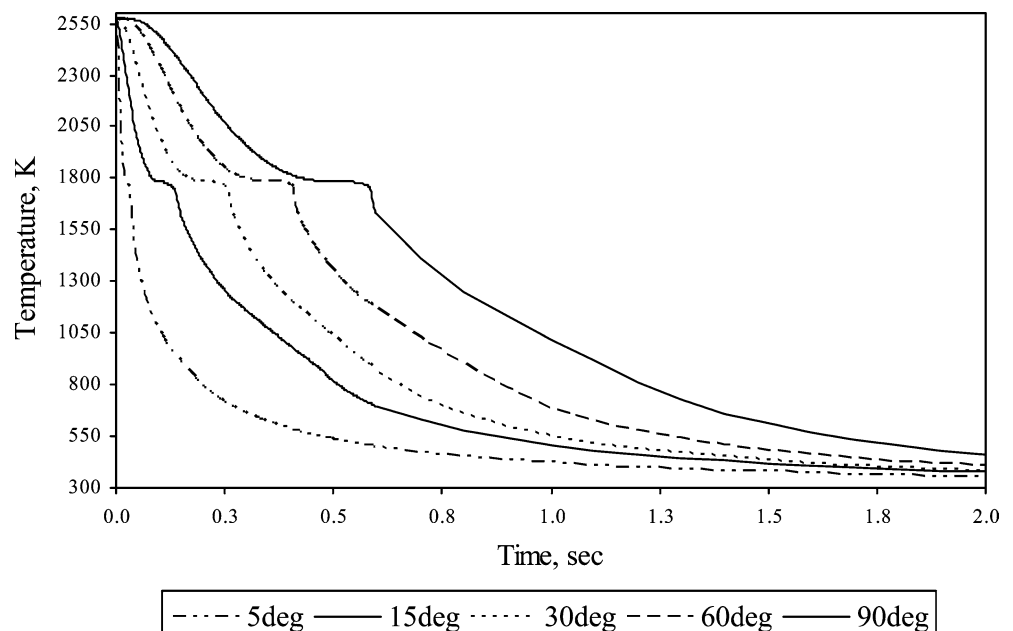


**Fig. 6** Variation of solidification time with contact length

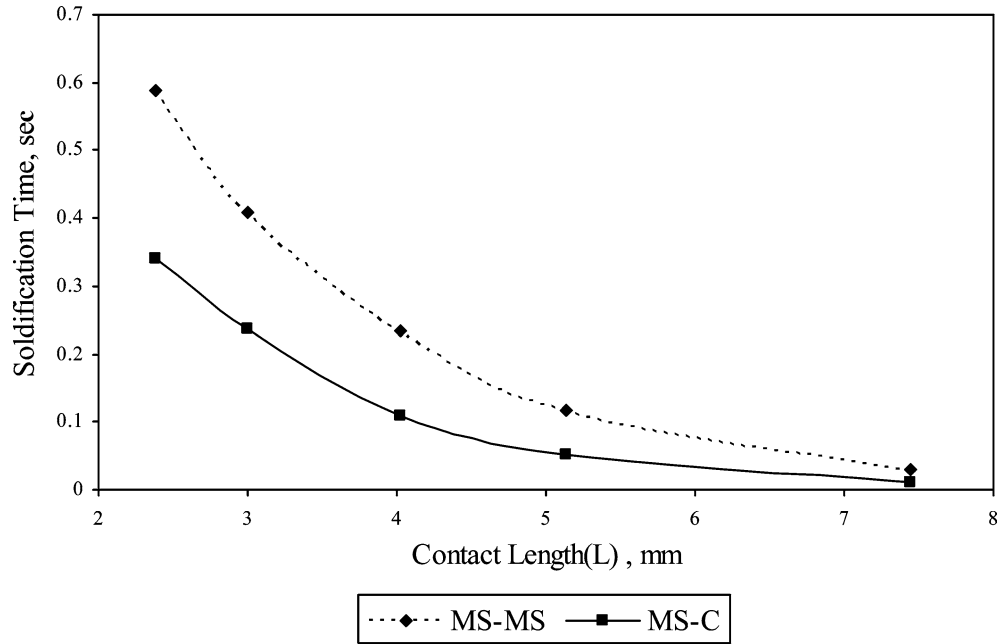
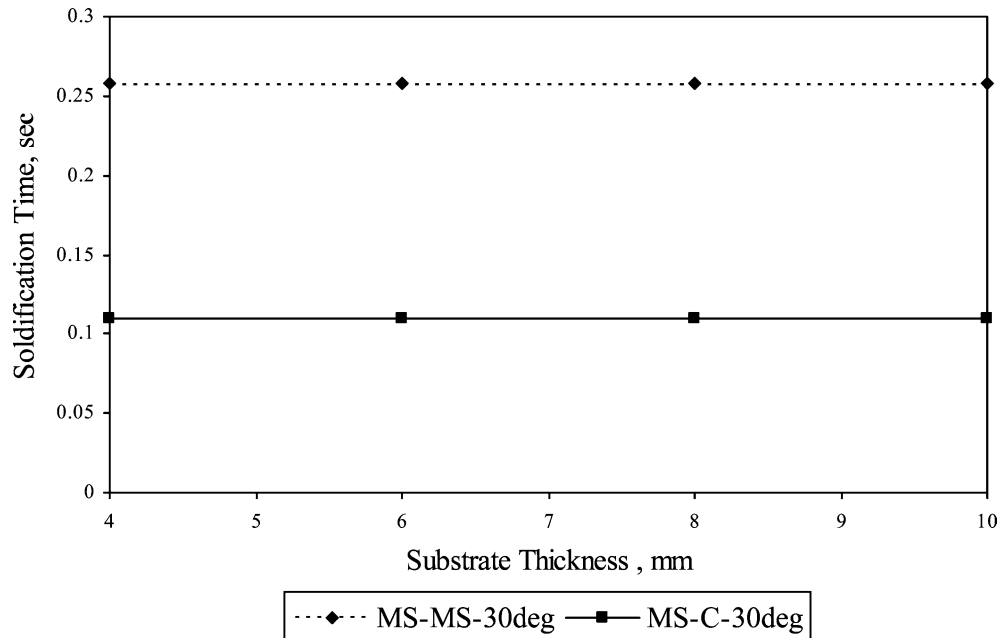


**Fig. 7** Variation of solidification time with substrate thickness



the cooler substrate reaches the top of the droplet with a time lapse, therefore the top portion of the curves, around 2,573 K, is flat for large contact angles but for small contact angles as soon as the droplet comes in contact with the substrate the top of the droplet starts losing heat. The reason for this is the ratio of height of the droplet to contact length, for large  $H/L$  ratio the thermal resistance is so large that the effect of heat sink appears with a time lapse.

The shape of the droplet and the thermal properties of the substrate have a significant effect on the solidification time of the droplet as shown in Fig. 6. It is clear that when the contact angle is small the solidification time is also small, this is because the contact length is

very large as compared to the droplet height or the  $H/L$  ratio is very large resulting in greater heat transfer area and the droplet loses its heat very quickly. The solidification time for an MS substrate is large compared to that of C substrate due to the large thermal diffusivity of C but for droplet shape with large contact length the effect of thermal properties will become less dominant as the two curves approach each other. The other process variables like the substrate size and the thermal boundary conditions do not have any effect on the solidification times as shown in Fig. 7. The reason for this behavior is the fact that this is a rapid solidification process and the heat wave does not penetrate enough into the substrate to have any significant effect.

**Fig. 8** Fourier number and dimensionless length

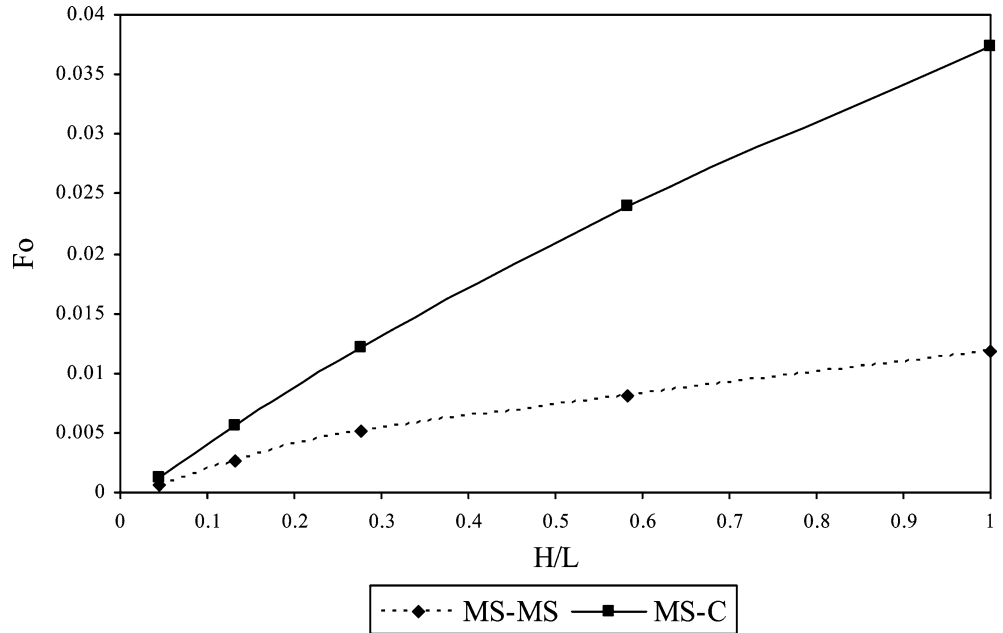


**Fig. 9** Steady-state time versus contact length for similar material interface

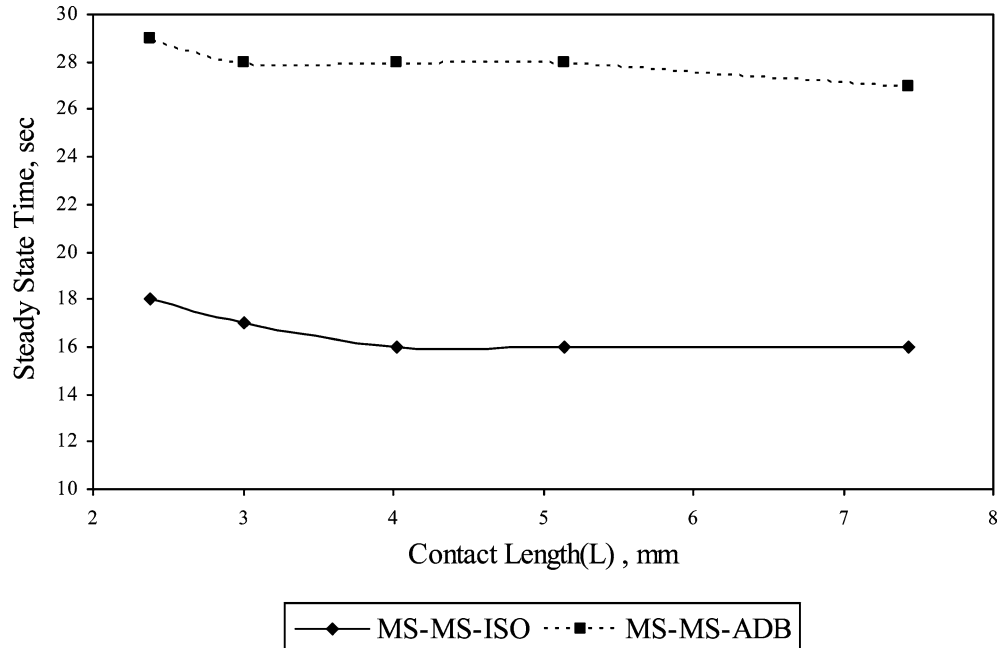


Figure 8, shows a plot between non-dimensional length, chosen as the ratio of droplet height ( $H$ ) to contact length ( $L$ ), and the Fourier number based on substrate thickness and solidification time. The Fourier number is given as

$$Fo = \frac{t_s \alpha}{st^2} \tag{6}$$

The Fourier number compares a characteristic body dimension, which in this case is the substrate thickness, with an approximate temperature wave penetration

depth for a given time  $t_s$ , which is the solidification time. It is very evident that, generally, due to high-thermal diffusivity the C substrate has large penetration depth compared to the MS substrate but for small contact angles this effect diminishes since at small contact angles the contact length is the controlling parameter rather than the thermal properties.

The control of residual stresses and deformations are essential in almost all the SFF processes especially those employing direct metal deposition like welding and microcasting. The rate at which the deposited metal cools down to room temperature can be an important



**Fig. 10** Steady-state time versus contact length for dissimilar material interface

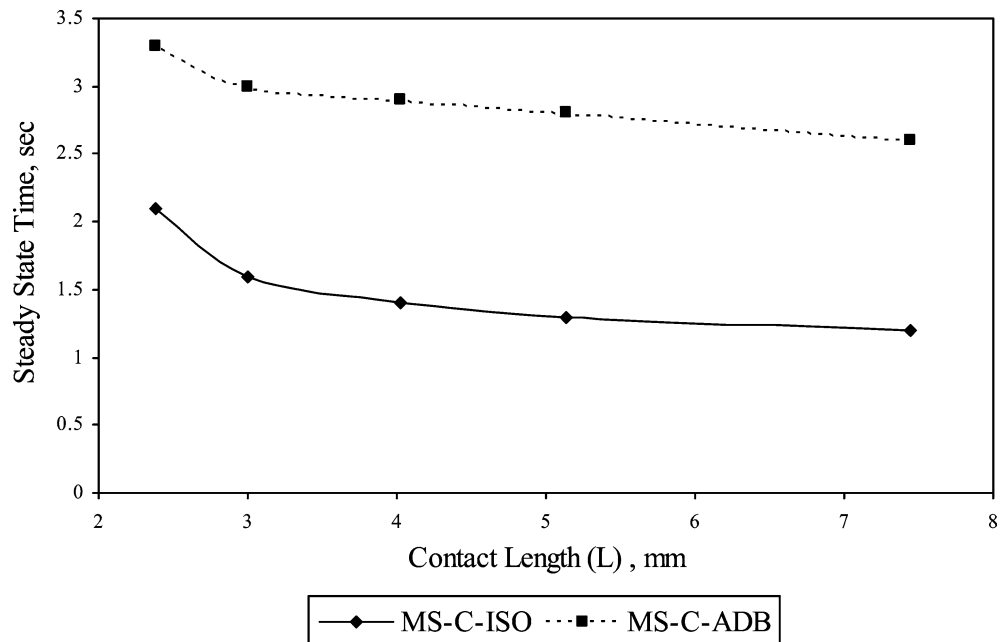
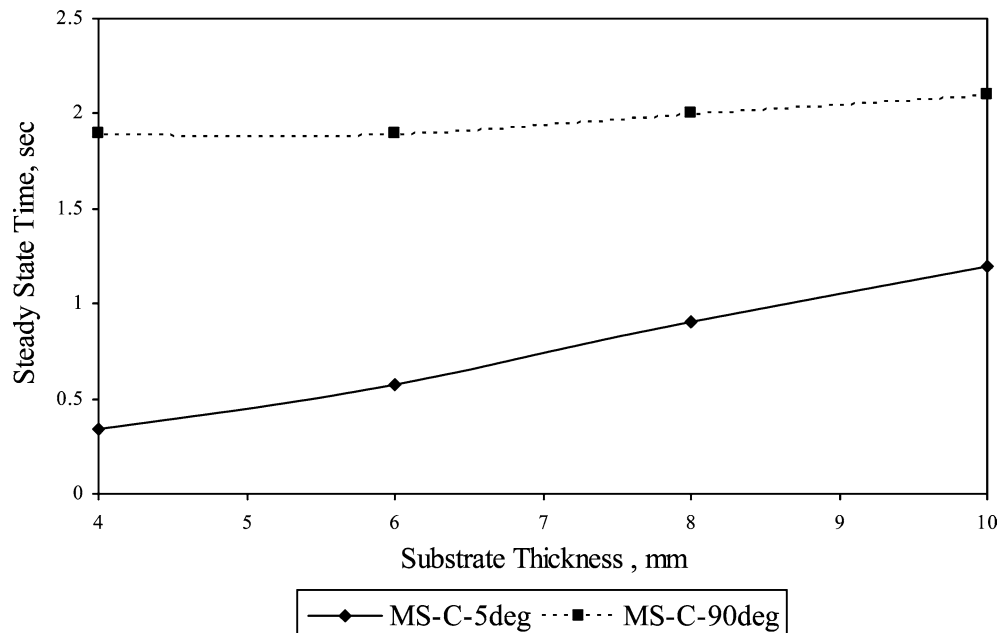


**Fig. 11** Variation of steady-state time with isothermal boundary conditions and dissimilar material interface



parameter in the buildup of residual stresses and deformations. Simulations were conducted to estimate the steady state of droplet-substrate domain and to observe the effect of different parameters on the steady-state time. It has been observed that droplet shape does not have any significant effect on steady-state time as compared to other process parameters like substrate thickness, thermal properties of the substrate and thermal boundary conditions.

As shown in Figs. 9 and 10, the variation of steady-state time with contact length is minor; the only significant variation observed is in the region of small contact length. The substrate with adiabatic base

shows large steady-state time as compared to isothermal base, which is logical since isothermal base gives low resistance to heat flow than the adiabatic base, and by reducing the cooling rate the adiabatic base will be helpful in controlling the buildup of residual stresses and deformations. Moreover, due to high-thermal diffusivity the C base shows much less steady-state time as compared to MS substrate. The steady-state time for a C substrate is almost ten times that of the C substrate.

The effect of substrate thermal properties and size with Isothermal boundary conditions at the base are shown in Figs. 11 and 12. It is evident that for C sub-

**Fig. 12** Variation of steady-state time with isothermal boundary conditions and similar material interface

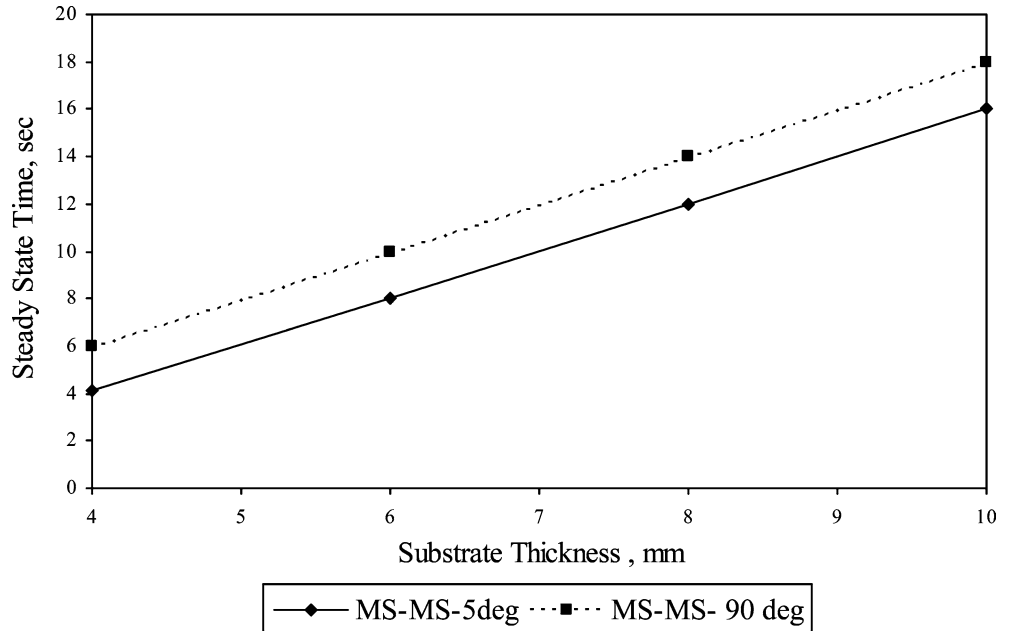
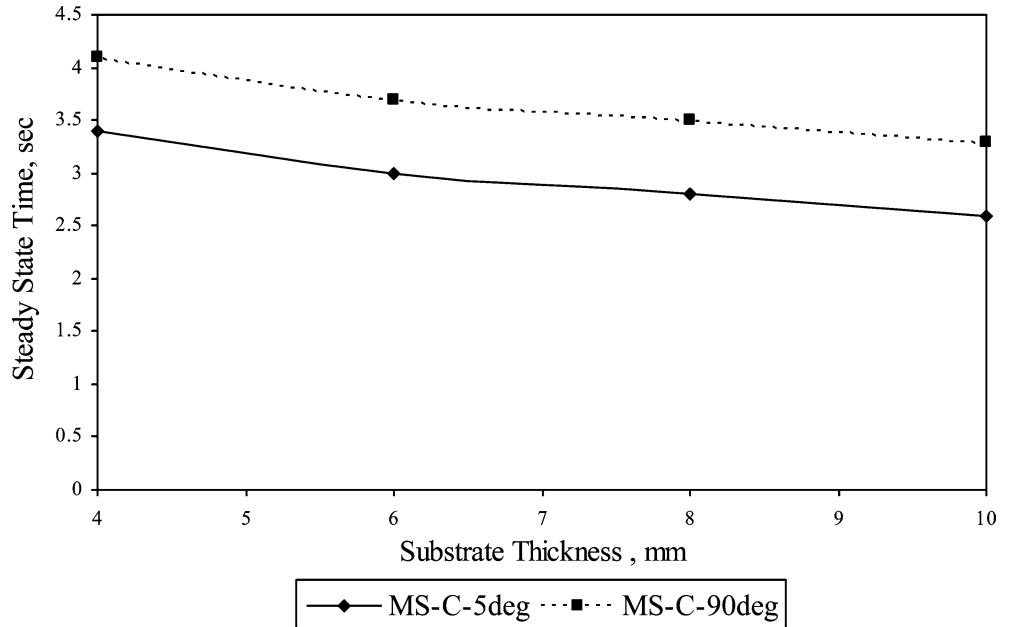


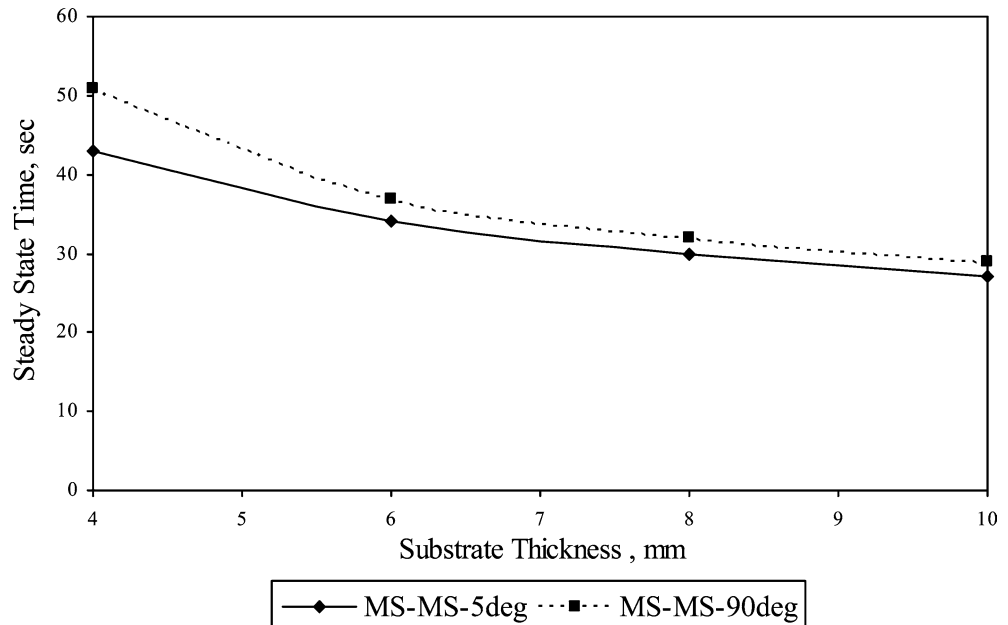
**Fig. 13** Variation of steady-state time with adiabatic boundary conditions and dissimilar material interface



strate the steady-state time for small contact angle varies significantly with changing substrate thickness but no such variation is evident for a higher contact angle droplet of 90°, where the steady-state time becomes independent of substrate thickness as shown in Fig. 11, however, for a MS substrate, Fig. 12, the trend of both the angles is similar that is of increasing steady-state time with substrate thickness. This behavior shows that by selecting a thick substrate the deformations and residual stresses can be reduced if isothermal conditions are obtained at the base. The effects of substrate thermal properties and size with adiabatic boundary conditions at the base are shown in Figs. 13 and 14. Both the plots

show that steady-state time decreases with increasing substrate thickness as the adiabatic base provides high resistance to heat flow as compared to the isothermal base but in comparison with an isothermal base the overall steady-state time increases. Generally, adiabatic base results in an increase of steady-state time by 80% as compared to isothermal base, but for small substrate thickness the increase can be as large as 600%, this is evident when Figs. 12 and 14 are compared. This large variation shows that by proper insulation the residual stresses and deformations can be reduced. Figure 14 shows that for substrates with low-thermal diffusivity the two curves come very close to each other showing

**Fig. 14** Variation of steady-state time with adiabatic boundary conditions and similar material interface



that with a substrate of low-thermal diffusivity and large thickness the shape of the droplet do not have any significant effect on the steady-state time.

## 9 Conclusion

In this paper, a comprehensive study has been conducted to predict the effect of droplet shape on the solidification and overall cooling of a molten metal droplet and also to study the effect of substrate size, thermal properties and substrate base boundary conditions on the cooling rate. It has been observed that the contact angle variation significantly affect the solidification time, whereas the substrate thickness does not affect the solidification time as the process is very rapid and the heat affected zone lies very near the droplet-substrate interface, but when the analysis is extended further to steady-state condition then the heat sink size affects the overall cooling rate. The effect of contact angle, as compared to thermal properties, boundary conditions and substrate size, is not very significant on steady-state time. The change in the cooling rate brought about by thermal insulation of the base is appreciable and can be used to control the build of residual stress and deformation.

## References

1. Merz R (1994) Shape deposition manufacturing, PhD. Dissertation eingereicht an Technischen Universität Wien
2. Amon CH, Beuth JL, Weiss LE, Mertz R, Prinz FB (1998) Shape deposition manufacturing with microcasting: processing, thermal and mechanical issues. *ASME J Manuf Sci Eng* 120:656–665
3. Trapaga G, Matthys EF, Valencia JJ, Szekeley J (1992) Fluid flow, heat transfer and solidification of a molten metal droplet impinging on substrates: comparison of numerical and experimental results. *Metall Trans B* 23:700–718
4. Bertagnolli M, Marchese M, Jacucci M, Doltsinis G, Noelting S (1994) Finite element thermo-mechanical simulation of droplets impacting on a rigid substrate. In: Proceedings of the energy technological conference and exhibition, ASME symposium on materials, design and analysis, ETCE. New Orleans, LA, vol 8, pp1591–1602
5. Kang B, Zhao, Poulikakos D (1994) Solidification of liquid metal droplets impacting sequentially on a solid surface. *ASME Trans J Heat Transf* 116:436–445
6. Xin J, Megaridis CM (1995) Calculation of tandem droplet array evaporating near a vertical hot plate. *Numer Heat Transfer A* 27:211–228
7. Attinger D, Poulikakos D (2001) Melting and re-solidification of a substrate caused by molten micro-droplet impact. *Trans ASME JHeat Transfer* 123:1110–1122
8. Haferi S, Butty V, Poulikakos D, Giannakouros J, Boomsma K, Megaridis CM, Nayagam V (2001) Freezing dynamics of molten solder droplets impacting onto flat substrates in reduced gravity. *Int J Heat Mass Transfer* 44:3513–3528
9. Haferi S, Poulikakos D (2002) Transport and solidification phenomena in molten micro-droplet pileup. *J Appl Phys* 92(2):1675–1689
10. Amon CH, Merz FB, Prinz R, Schmaltz KS (1994) Thermal modeling and experimental testing of MD spray shape deposition processes. In: Proceedings of the 10th international heat transfer conference. Brighton, UK
11. Amon CH, Schmaltz KS, Merz FB, Prinz R (1996) Numerical and experimental investigation of interface bonding via substrate remelting of an impinging molten metal droplet. *ASME Trans J Heat Transfer* 118:164–172
12. Chin RK, Beuth JL, Amon CH (1996) Droplet level modeling of thermal stresses in layered manufacturing methods. In: ASME international mechanical engineering congress. Atlanta, GA, pp17–22
13. Chin RK, Beuth JL, Amon CH (2001) Successive deposition of metals in SFF processes, Part1: thermo mechanical models of layers and droplet columns. *J Manuf Sci Eng* 3:623–631
14. Chin RK, Beuth JL, Amon CH (2001) Successive deposition of metals in SFF processes, Part2: thermo mechanical models of adjacent droplet. *J Manuf Sci Eng* 123:632–638

15. Zarzalejo LJ, Schmaltz KS, Amon CH (1999) Molten droplet solidification and substrate remelting in microcasting. Part1: numerical modeling and experimental verification. *Heat Mass Transf* 34:477–485
16. Schmaltz KS, Zarzalejo LJ, Amon CH (1999) Molten droplet solidification and substrate remelting in microcasting. Part2: parametric study and effect of dissimilar materials. *Heat Mass Transf* 35:17–23
17. Karlson RI, Josefson BL (1990) Three dimensional finite element analysis of temperature and stresses in a single pass butt-welded pipe. *ASME Trans* 112:76–83
18. Bushko W, Grosse IR (1991) New finite element method for multi dimensional heat transfer problem. *Numer Heat Transfer B* 19:31–48
19. Lide DR (1991–92) *CRC handbook of chemistry and physics*, 72nd edn. CRC Press, Boca Raton